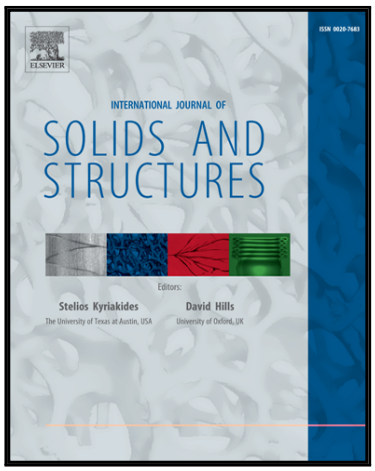

Explicit, comprehensive modeling of multi-axial finite strain pseudo-elastic SMAs up to failure

H. Xiao, X.M. Wang, Z.L. Wang, Z.N. Yin

PII: S0020-7683(16)00125-6
DOI: 10.1016/j.ijsolstr.2016.03.006
Reference: SAS 9094

To appear in: *International Journal of Solids and Structures*

Received date: 30 October 2015
Revised date: 2 March 2016
Accepted date: 9 March 2016

Please cite this article as: H. Xiao, X.M. Wang, Z.L. Wang, Z.N. Yin, Explicit, comprehensive modeling of multi-axial finite strain pseudo-elastic SMAs up to failure, *International Journal of Solids and Structures* (2016), doi: 10.1016/j.ijsolstr.2016.03.006

Explicit, comprehensive modeling of multi-axial finite strain pseudo-elastic SMAs up to failure

H. Xiao[1], X.M. Wang[1], Z.L. Wang[1,2], Z.N. Yin[1]

1.State Key Laboratory for Advanced Special Steels (Shanghai University) and Shanghai Institute of Applied Mathematics and Mechanics, Yanchang Road 149, 200072 Shanghai, China

2. College of Mathematics and Information Sciences, Weifang University, Weifang 261061, Shandong Province, China

Abstract

A new elastoplastic J_2-flow model with nonlinear combined hardening is proposed for the purpose of achieving an explicit, comprehensive simulation of pseudo-elastic SMAs over the whole range of strain up to failure. To this goal, a new, explicit methodology based on any given uniaxial data is introduced to obtain multi-axial expressions for the constitutive quantities incorporated in this model, in such a unified sense that all three successive deformation stages may be simultaneously represented, including a pseudo-elastic stage with perfect strain recovery, a hardening stage with partial strain recovery, and a softening stage up to failure. As such, any given shapes of uniaxial stress-strain curves from both loading and unloading in these three stages may be automatically reproduced from the proposed model, without involving usual complicated numerical procedures in treating nonlinear rate

Email address: xiaoheng@shu.edu.cn (H. Xiao[1])

constitutive equations with a number of switching conditions. Numerical examples with test data are supplied to simulate a complete process including all three stages.

Keywords: Shape memory alloys, Pseudoelasticity, Plasticity, Softening, Failure behavior, Explicit approach

1. Introduction

When subjected to strain within a certain range, a pseudo-elastic SMA sample is known to display strain recovery effect upon unloading. However, such recovery effect may not be maintained and, accordingly, irrecoverable strain upon unloading may be expected, whenever strain at loading exceeds the foregoing range. In further development of straining, softening effect is expected and failure eventually takes place. Such three successive stages of distinct SMA inelastic behaviors over the whole range of strain up to failure are schematically shown in Fig. 1 in §2.4 for uniaxial stress-strain curves when unloading occurs within different ranges of strain.

Toward modeling pseudo-elastic SMAs in a comprehensive sense, the foregoing three successive stages need to be simultaneously represented by establishing suitable constitutive models in unified form. Such unified models for all deformation stages of pseudo-elastic SMAs up to failure are of significance but have long been unavailable to date.

In the past decades, numerous studies have been made in modeling pseudo-elastic SMAs. Usually, attention has been confined to the pseudo-elastic stage in the foregoing. Starting from phase transition mechanisms between martensite and austenite, results have been derived from either microscopic or

mesoscopic or phenomenological standpoints. Recent surveys in these three respects may be found in the review articles by Patoor et al. (2006) and Lagoudas et al. (2006), as well as in relevant monographs, e.g., by Auricchio (1995), Battacharya (2003) and Lagoudas (2010). In particular, extensive studies in the significant respects of microscopic and mesoscopic models may be found in the just mentioned references and the references therein. Here our interest is in the respect of phenomenological (macroscopic) models in a direct sense. Some representative samples of recent contributions in this respect are briefly discussed below.

Firstly, extensive studies have been devoted to modeling the pseudo-elastic hysteresis. Earlier, a simple polynomial potential model with a Landau-Devonshire free-energy function was proposed by Falk (1980) for some simple cases. A four-parameter model based also on a Landau-Devonshire free-energy was suggested by Huo (1989) in a further study. In a recent development, a microplane model has been presented by Brocca et al. (2002) (cf., Mehrabi et al. 2014) by developing a slip theory for polycrystal plasticity. Yu et al. (2014b) propose a new crystal plasticity constitutive model for rate-dependent development of SMAs. Moreover, another approach in wide application, initiated by Tanaka and Nagaki (1982), is based on introduction of various internal variables in an averaged sense of representing microstructural features relating to the martensite-austenite phase transitions. Numerous results for small strain cases may be found in the aforementioned review articles and monographs and the references therein. Here, for results prior to 2006, attention is directed to finite strain cases; refer to, e.g., Tanaka (1987); Auricchio and Taylor (1997); Masud et al. (1997); Auricchio (2001); Helm

and Haupt (2003); Peng et al. (2001); Shaw (2002), Lexcellent et al. (2006). Most recent developments are concerned with multi-axial modeling and results may be found in, e.g., Popov and Lagoudas (2007), Peng et al. (2008); Arghavani et al. (2010a), Morin et al. (2011), Saleeb et al. (2011), Yu et al. (2013) for small strain cases, and Müller and Bruhns (2006), Helm (2007), Ziólkowski (2007), Luig and Bruhns (2008), Thambujara (2010), Arghavani et al. (2011), Teeriaho (2013) for finite strain cases. Further studies in treating martensite reorientation are given in, e.g., Panico and Brinson (2007); Arghavani et al. (2010b), Zaki (2012), Yoo et al. (2015) and others. Some most rcent results with numerical implementations may be found in, e.g., Vidyashankar et al. (2007), Moumni et al. (2008); Reese and Christ (2008); Hartl et al. (2010); Arghavani et al. (2011), Lagoudas et al. (2012).

Next, further results in simulating two stages with complete and partial strain recovery are presented, e.g., in Paiva et al. (2005) and Auricchio et al. (2007) for cases coupled with permanent inelasticity and in Yu et al. (2013) for a simulation based on microstructural mechanisms, as well as in Hartl et al. (2009), Zhou (2012), Yu et al. (2014a) and many others.

On the other hand, the localization and fracture behavior of shape memory alloys are studied in, e.g., Shaw and Kyriakides (1997, 1998), Desindes and Daly (2010), Maletta and Furgiuele (2011), Hallai and Kyriakides (2013). These studies are concerned with the structural instability and failure of SMAs.

In the existing studies of SMA modeling as briefly summarized in the above, it is customary to derive results from various standpoints based on solid-solid phase transition mechanisms between austenite and martensite.

Irrespective of the fact that numerous significant results are available in the past decades, it appears that rigorous and reliable continuum-level constitutive models do not exist and need to be developed to meet requirements for efficient engineering applications of SMAs. Although the understanding based on the micromechanical aspects of phase transformation mechanisms has arrived at a comfortable level, nevertheless the quantitative connection between microscopic and macroscopic behavior prove to be undue complex and has not yet been developed to the degree required by such continuum-level models as mentioned in the foregoing. Most recently, it has been demonstrated (Xiao et al. 2010a,b, 2011; Xiao 2013, 2014a; Wang et al. 2014) that elastoplastic J_2-flow models just in the continuum-level sense may be established to simulate SMA thermomechanical behaviors in an explicit, direct sense without involving any phase variables. Explicit results have been obtained for SMA pseudo-elastic behavior with any given shape of hysteresis loops (Xiao 2013, 2014a; Wang et al. 2014).

In this contribution, we are going to show that a new elastoplastic J_2-flow model may be established to accomplish an explicit, comprehensive simulation of all three deformation stages of pseudo-elastic SMAs over the whole range of strain up to failure. It will be shown that explicit expressions for the constitutive quantities introduced, including the hardening moduli and the yield strength, may be presented in such a unified sense that all the three successive stages described before may be simultaneously represented. As such, any given shapes of uniaxial stress-strain curves from both loading and unloading in respective stages, as shown in Fig. 1 in §2.4, may be automatically, exactly reproduced from the proposed model, without involv-

ing usual complicated numerical procedures in treating systems of nonlinear rate constitutive equations with a number of switching conditions as well as micro-to-macro averaged procedures.

The main content of this article will be arranged as follows. In Section 2, new elastoplastic J_2-flow models with nonlinear combined hardening will be introduced, in conjunction with a brief description of all three stages of pseudo-elastic SMAs up to failure. In the next two sections, viz. Sections 3 and 4, results will be presented separately for three successive stages, including a pseudo-elastic stage with perfect strain recovery, a hardening stage with partial strain recovery, as well as a softening stage up to failure. In Section 5, results in Sections 3 and 4 will be combined to yield unified results for all the three stages. In Section 6, numerical results with test data will be supplied to reproduce a complete process from the initial straining to failure, where typical unloading responses occurring in the foregoing three stages are incorporated. Finally, novelties of the proposed model will be explained in comparison with various usual models and further developments will be indicated in Section 7.

2. Elastoplastic J_2-flow models with substantial coupling

We direct attention to the consistent Eulerian formulation of finite elastoplasticity, developed in recent years (see, e.g., Xiao et al. 2006, 2007). In a most recent study (Xiao 2013, 2014a), finite strain elastoplastic J_2-flow models have been established to achieve an explicit, direct simulation of pseudo-elastic SMAs. A departure from usual elastoplastic models is that a general case of combined hardening with a yield strength relying both on the

plastic work and on the the back stress should be introduced in a sense of coupling the changing of the size of the yield surface with the moving of the yield surface center. The new model introduced below may be established following the procedures in Xiao (2014a), in which the usual plastic work is replaced by the effective plastic work. Here, such procedures are omitted and details may be found in the foregoing reference.

Here and henceforth, $\boldsymbol{F}$ and $\boldsymbol{D}$ are used to denote the deformation gradient and the stretching and $\boldsymbol{\tau}$ stands for the Kirchhoff stress, i.e. the Cauchy stress $\boldsymbol{\sigma}$ weighted by the deformation Jacobian $J = \det\boldsymbol{F}$ and then $\boldsymbol{\tau} = J\,\boldsymbol{\sigma}$. The deviatoric part of the latter is denoted $\tilde{\boldsymbol{\tau}}$. Throughout, the superimposed dot means the material time derivative.

The starting point is to assume that the stretching $\boldsymbol{D}$ for finite elasto-plastic deformations is formed by an elastic part, $\boldsymbol{D}^e$, and a plastic part, $\boldsymbol{D}^p$, namely (cf., Khan ang Huang 1995)

$$\boldsymbol{D} = \boldsymbol{D}^{\mathrm{e}} + \boldsymbol{D}^{\mathrm{p}}\,. \tag{1}$$

Objective rate constitutive equations should be prescribed for the two parts in the above decomposition, as will be done below, separately.

2.1. Elastic rate equation

Firstly, the elastic part $\boldsymbol{D}^e$ is assumed to be governed by the following elastic rate equation of hypoelastic type:

$$\boldsymbol{D}^{\mathrm{e}} = \frac{1+\nu}{E}\ \overset{\circ}{\boldsymbol{\tau}} - \frac{\nu}{E}\,(\mathrm{tr}\,\overset{\circ}{\boldsymbol{\tau}})\,\boldsymbol{I}\,. \tag{2}$$

In the above, $\overset{\circ}{\boldsymbol{\tau}}$ is the co-rotational logarithmic rate of the Kirchhoff stress $\boldsymbol{\tau}$ and of the form

$$\overset{\circ}{\boldsymbol{\tau}} = \dot{\boldsymbol{\tau}} + \boldsymbol{\tau} \cdot \boldsymbol{\Omega} - \boldsymbol{\Omega} \cdot \boldsymbol{\tau} \,, \tag{3}$$

where $\boldsymbol{\Omega}$ is the logarithmic spin (cf., e.g. Xiao et al. 1997), and, moreover, $\boldsymbol{I}$ is the second-order identity tensor.

2.2. Plastic flow rule with substantial coupling

Next, the plastic part $\boldsymbol{D}^p$ is governed by the normality flow rule (cf. Bruhns et al. 2005):

$$\boldsymbol{D}^{\mathrm{p}} = \frac{\xi}{u} \left(\frac{\partial f}{\partial \boldsymbol{\tau}} : \overset{\circ}{\boldsymbol{\tau}} \right) \frac{\partial f}{\partial \boldsymbol{\tau}} \,. \tag{4}$$

As in Eq. (2), $\overset{\circ}{\boldsymbol{\tau}}$ is the corotational logarithmic rate of the Kirchhoff stress $\boldsymbol{\tau}$. Use of the latter ensures that both the elastic and the plastic rate equations (2) and (4) fulfill certain consistency requirements. Details in this respect may be found in, e.g., Bruhns et al. (1999, 2003), Xiao et al. (2000a,b), and Xiao et al. (2006).

The plastic indicator ξ takes values 1 and 0 in the loading and unloading cases, respectively, as given in Bruhns et al. (2003). The plastic modulus u will be given slightly later.

The yield function f in Eq. (4) is taken to be of von Mises type:

$$f = \frac{1}{2} \, \mathrm{tr}(\tilde{\boldsymbol{\tau}} - \boldsymbol{\alpha})^2 - \frac{1}{3} \, r^2 \,. \tag{5}$$

In the above, the yield strength r prescribes the radius of the current yield surface $f = 0$ and the back stress $\boldsymbol{\alpha}$ specifies the center of the current yield

surface $f = 0$. In general, both of them are changing in development of plastic flow and such changes just characterize combined hardening behavior.

Usually, it is assumed that there is no coupling between the changing of the yield strength r (i.e., the size of the current yield surface) and the moving of the yield surface center. Most recently (Xiao 2014a), it has been found that coupling between the latter two may play a substantial role in modeling pseudo-elastic hysteresis. Here, the yield strength r is taken to be dependent on both the effective plastic work $\tilde{\kappa}$ and the back stress $\boldsymbol{\alpha}$ as shown below:

$$r = r(\tilde{\kappa}, \zeta) > 0\,, \tag{6}$$

with the effective plastic work:

$$\dot{\tilde{\kappa}} = (\tilde{\boldsymbol{\tau}} - \boldsymbol{\alpha}) : \boldsymbol{D}^{\mathrm{p}} \tag{7}$$

and the magnitude of the back stress:

$$\zeta = \sqrt{\mathrm{tr}\boldsymbol{\alpha}^2}\,. \tag{8}$$

It should be pointed out that here the introduction of the effective plastic work (cf., Eq. (7)) represents a new development of the model in the previous study (Xiao 2014a). The latter is based on the usual plastic work below:

$$\kappa = \boldsymbol{\tau} : \boldsymbol{D}^{p}\,.$$

It may be noted that the effective plastic work $\tilde{\kappa}$ is monotonically increasing with development of plastic flow, whereas that may not be the case for the plastic work κ. These two agree with each other only in the absence of anisotropic hardening.

2.3. Nonlinear combined hardening

The traceless back stress $\boldsymbol{\alpha}$ is governed by the following new nonlinear anisotropic hardening rule:

$$\overset{\circ}{\boldsymbol{\alpha}} = c\,\boldsymbol{D}^{\mathrm{p}} - \frac{\gamma}{r}\,\dot{\tilde{\kappa}}\,\boldsymbol{\alpha}\,, \tag{9}$$

with

$$c = c(\tilde{\kappa}, \zeta), \quad \gamma = \gamma(\tilde{\kappa}, \tilde{\boldsymbol{\tau}}, \boldsymbol{\alpha})\,. \tag{10}$$

On account of certain consistency requirements, it has been demonstrated (cf. Xiao et al. 2000a) that the objective rate $\overset{\circ}{\boldsymbol{\alpha}}$ in Eq. (9) should also be the co-rotational logarithmic rate.

Now the plastic modulus u in Eq. (4) is given as follows:

$$u = \frac{2}{3}cr^2 + \frac{4}{9}r^3 r' - \frac{4}{9}\gamma\, r^2\, \bar{r}'\zeta + \frac{2}{3}r\left(1.5c\,\bar{r}'\zeta^{-1} - \gamma\right)(\tilde{\boldsymbol{\tau}} - \boldsymbol{\alpha}) : \boldsymbol{\alpha}\,. \tag{11}$$

Here and henceforth, the following notations are used:

$$r' = \frac{\partial\, r}{\partial\, \tilde{\kappa}}, \quad \bar{r}' = \frac{\partial r}{\partial \zeta}\,. \tag{12}$$

In the above, a new nonlinear combined hardening J_2-flow model has been established with coupling effects between the changing of the size of the yield surface and the moving of the yield surface center. Its thermodynamic consistency may be treated following the procedures in § 2.2 in Xiao (2014a).

It has been shown in a previous study (Xiao 2014a) that suitable forms of the hardening moduli c and γ as well as the yield strength r may be explicitly given for the purpose that SMA pseudo-elastic behavior with any given shape of hysteresis loops may be simulated. In fact, explicit expressions

for the former are obtainable in terms of certain shape functions specifying pseudo-elastic hysteresis loops. In the subsequent development, we are going to show that further results may be presented for the purpose of achieving an explicit, comprehensive simulation of all three deformation stages of pseudo-elastic SMAs up to failure.

2.4. Three stages of SMA uniaxial behavior up to failure

Consider a peudoelastic SMA sample that undergoes uniaxial straining. As indicated at the outset of the introduction section, three stages of distinct deformation behaviors may be expected, including a pseudo-elastic stage with perfect strain recovery, a hardening stage with partial strain recovery and a softening stage up to failure, as shown in Fig. 1. In Fig. 1, the upper stress-strain curve is generated in a monotonically straining process from an initial state up to failure and referred to as the primary plastic curve. An unloading process at each point on the primary plastic curve produces a stress-strain curve starting at this point. For a pseudo-elastic SMA sample, a new understanding from the standpoint of classical elastoplasticity is that a subsequent yield point may emerge above the strain axis, thus leading to subsequent plastic flow just in the unloading process. Each such curve is named a subsequent plastic curve. The three stages at issue correspond with the three parts of the primary plastic curve, including a slowly rising part from point A to point B and a relatively fast rising part from point B to point C as well as a softening part falling down from point C toward the strain axis.

At the pseudo-elastic stage, hysteresis loops will be generated by loading-unloading processes. A typical loop, i.e. OP^*P_*O, is shown in Fig. 1, where

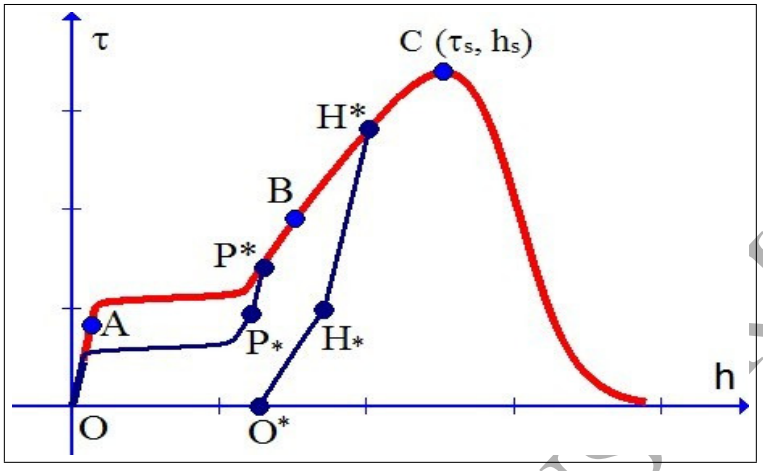

Figure 1: Three stages for deformation behavior of pseudo-elastic SMAs

P^* and P_* are the unloading point and the subsequent yield point. At the hardening stage, however, no loops will be produced by loading-unloading processes. A typical stress-strain curve, $OH^*H_*O_*$, is shown in Fig. 1, where H^* and H_* are the unloading point and the subsequent yield point and, moreover, O_* is the point at the end of unloading. A marked difference may be noted, namely, at the end of unloading, the former produces negligibly small irrecoverable strain, whereas the latter gives appreciable irrecoverable strain.

The elastic part P^*P_* or H^*H_* is given by

$$\tau - \tau^* = E(h - h^*)\,, \tag{13}$$

where τ^* and h^* are the axial Kirchhoff stress and Hencky's logarithmic strain at point P^* or H^*. The slope of the elastic part is given just by the Young's modulus E.

One of the main issues in modeling SMAs is to establish a comprehensive

constitutive model that can simultaneously simulate the above three stages of distinct inelastic behaviors, in a broad sense with any given shapes of the primary plastic curve $OABC$ and the subsequent plastic curves P^*P_*O and $H^*H_*O_*$ for both stages with perfect and partial recovery, as well as the softening part up to failure.

Suitable test dada should be given for each of the above curves. Constitutive models are then established to fit test data as closely as possible. Usually, each such model is given by a strongly coupled system of nonlinear rate type constitutive equations with a number of unknown parameters incorporated, in conjunction with certain switching rules associated with various cases of phase transition mechanisms between austenite and martensite. As such, the unknown parameters have to be identified implicitly by complicated numerical procedures of treating a coupled system of nonlinear equations in fitting test data and such procedures would have to be repeatedly carried out for data sets for different samples.

We are going to show that an explicit, direct approach to modeling SMAs is possible. Toward this objective, in the succeeding sections the hardening moduli c and γ as well as the yield strength r will be presented explicitly in terms of certain shape functions prescribing the primary plastic curve and the subsequent plastic curves in Fig. 1, in the sense that any given shapes of the latter may be automatically reproduced.

In the sequel, results will be derived first for each of the foregoing three stages, separately, and, then, these results will be combined into a unified form for all the stages.

3. Pseudo-elastic stage with perfect strain recovery

In this section, we are going to present explicit expressions for c, γ and r in terms of the shape functions for the primary and subsequent plastic curves. Results in this respect have been obtained in a previous study (Xiao 2014a) based on the usual plastic work. Here, results may be derived for the new model following the same procedures. Detail will no longer be given and may be referred to the foregoing reference.

3.1. Shape functions for the primary and subsequent plastic curves

Toward our purpose, the two curves at issue will be represented by two shape functions described below. On the one hand, a strain-stress function is given to prescribe the primary plastic curve, namely,

$$\overline{h} = p(\overline{\tau}), \quad p(r_0) = \frac{r_0}{E}\,. \tag{14}$$

Given suitable test data for the primary plastic curve, the above function is obtainable either directly from usual interpolating approaches or from other approaches. In the above, r_0 is the intial yield strength at the initial yield point A (cf., Fig. 1), and $\overline{\tau}$ and $\overline{h}$ are the axial Kirchhoff stress and the axial Hencky strain at each point on the primary plastic curve (cf., Fig. 1).

On the other hand, a function below is given to specify the subsequent plastic curve in a hysteresis loop (cf., Fig. 1)

$$\overline{\tau} = \phi(\underline{\tau}), \quad \phi(0) = r_0\,. \tag{15}$$

The above function, named the bridging function for the primary and subsequent plastic curves, establishes the correlation between the axial stresses

$\overline{\tau}$ and $\underline{\tau}$ at each pair of primary and subsequent yield points linked by an elastic unloading line, as shown in Fig. 1. At the initial yield point A (cf., Fig. 1), we have $\overline{\tau} = r_0$. In particular, we have $\underline{\tau} = 0$ at the origin O. The latter is just the strain recovery condition at the origin O.

Eqs. (13)-(15) produce

$$\underline{h} = q(\underline{\tau}) \equiv p(\phi(\underline{\tau})) + \frac{1}{E}(\underline{\tau} - \phi(\underline{\tau})) \tag{16}$$

for the axial strain $\underline{h}$ and the axial stress $\underline{\tau}$ on the subsequent plastic curve. From this it follows that the subsequent plastic curve may be determined jointly by the shape function Eq. (14) and the bridging function Eq. (15). Detail may be referred to Xiao (2014a). Usually, it suffices to consider a linear bridging function below:

$$\overline{\tau} = b\underline{\tau} + r_0\,, \tag{17}$$

where $b > 0$ is a dimensionless parameter.

3.2. Plastic slope relations with multi-axial extension

From the constitutive equations established in the last section, two relations in the uniaxial case may be derived for the primary and subsequent plastic curves. Such relations relate the hardening moduli c and γ as well as the yield strength r to the geometric features of the two curves at issue. Then, each of the former is derivable from a multi-axial extension of these relations.

The axial stress τ on either the primary or the subsequent plastic curve may alternatively be reformulated as a function of the effective plastic work

$\tilde{\kappa}$. With this understanding, let τ' represent the derivative with respect to $\tilde{\kappa}$, namely, $\tau' = \frac{d\tau}{d\tilde{\kappa}}$ with $\tau = \tau(\tilde{\kappa})$. Then, the following relation may be derived:

$$\frac{1}{(\tau - \alpha)\tau'} = \frac{dh}{d\tau} - \frac{1}{E} \tag{18}$$

for either of the primary and subsequent plastic curves with $(\tau,\, h) = (\overline{\tau},\, \overline{h})$ and $(\tau,\, h) = (\underline{\tau},\, \underline{h})$. The combination $(\tau - \alpha)\tau'$ is referred to as the plastic slope of either of the two plastic curves.

By applying the constitutive equations in the last section, the plastic slope relations below may be derived (Xiao 2013, 2014a):

$$1.5c\left(1 + \zeta^{-1}\bar{r}'\Lambda\right) + r'r - \gamma(\Lambda + \bar{r}'\zeta) = \tau(\tau' - \alpha) = \begin{cases} \overline{K}(\overline{\tau})\,, \\ \underline{K}(\underline{\tau})\,, \end{cases} \tag{19}$$

for the primary and subsequent plastic curves, respectively, where

$$\Lambda = \frac{1.5}{r}(\tilde{\boldsymbol{\tau}} - \boldsymbol{\alpha}) : \boldsymbol{\alpha} \tag{20}$$

and the plastic slopes for the two plastic curves may be given by

$$(\overline{\tau} - \overline{\alpha})\,\overline{\tau}' = \overline{K}(\overline{\tau}) \equiv \frac{1}{p'(\overline{\tau}) - E^{-1}}\,, \tag{21}$$

$$(\underline{\tau} - \underline{\alpha})\,\underline{\tau}' = \underline{K}(\underline{\tau}) \equiv \frac{1}{q'(\underline{\tau}) - E^{-1}} = \frac{b^{-1}}{p'(b\underline{\tau} + r_0) - E^{-1}} \tag{22}$$

The two relations given by Eq. (19) are merely applicable to the uniaxial case. Toward obtaining results for general multi-axial cases, it may be essential to have an appropriate multi-axial extension of Eq. (19). Such an extension has been proposed in Xiao (2014a) and given below:

$$1.5c\left(1 + \zeta^{-1}\bar{r}'\Lambda\right) + r'r - \gamma(\Lambda + \bar{r}'\zeta) = K(\Lambda, r)\,, \tag{23}$$

where

$$K(\Lambda, r) \equiv \frac{[\Lambda + r]}{|\Lambda| + r} \overline{K}(|\Lambda| + r) + \left(1 - \frac{[\Lambda + r]}{|\Lambda| + r}\right) \underline{K}(|\Lambda| - r)\,, \tag{24}$$

with

$$[\Lambda + r] = \frac{1}{2}\left(\Lambda + r + |\Lambda + r|\right)\,.$$

In the uniaxial case, the multi-axial extension Eq. (24) exactly yields the two plastic slopes $\overline{K}(\overline{\tau})$ and $\underline{K}(\underline{\tau})$ (cf., Eqs. (21)-(22)) for the primary and subsequent plastic curves (cf., Fig. 1) and, therefore, Eq. (23) reduces to Eq. (19) in the uniaxial case. Moreover, the two plastic slopes given by Eqs. (21)-(22) may be extended to cover the whole range $(-\infty, +\infty)$ for the stress variable by assuming symmetry in tension and compression (Xiao 2014a). A general case with tension-compression asymmetry has been treated in Wang et al. (2014). Further discussion may be referred to these recent references.

3.3. Multi-axial anisotropic hardening moduli

Now the two hardening moduli c and γ may be derived from Eq. (23) following the procedures in Xiao (2013, 2014a). Results are as follows:

$$c = \frac{2}{3}\frac{K(-\zeta\bar{r}', r) - rr'}{1 - \bar{r}'^2}\,, \tag{25}$$

$$\gamma = \frac{1 + \zeta^{-1}\bar{r}'\Lambda}{(1 - \bar{r}'^2)(\Lambda + \bar{r}'\zeta)}(K(-\bar{r}'\zeta, r) - rr') + \frac{rr' - K(\Lambda, r)}{\Lambda + \bar{r}'\zeta} \tag{26}$$

with

$$\bar{r}'(\tilde{\kappa}, 0) = 0, \quad \bar{r}'^2 < 1\,. \tag{27}$$

The latter two ensure that multi-axial hardening moduli c and γ given above are well-defined for all possible cases.

3.4. Multi-axial yield strength

The yield strength r is of localized properties at both $\tilde{\kappa} = 0$ and $\zeta = 0$, as explained in the previous study (Xiao 2013, 2014a). Two localized terms may be introduced to characterize these localized properties. For a linear bridging function given by Eq. (17), result is given below:

$$r = \frac{b-1}{b+1}\sqrt{1.5}\zeta\left(1 - e^{-\varrho\frac{\zeta}{r_0}}\right) + \frac{r_0}{b+1}\left(1 + b\, e^{-\beta\frac{\tilde{\kappa}}{r_0}}\right), \tag{28}$$

where $\varrho > 0$ and $\beta > 0$ are two parameters characterizing the localized properties at $\zeta = 0$ and $\tilde{\kappa} = 0$. Note that the requirements specified by Eq. (27) are satisfied. Details may be found in Xiao (2013, 2014a). In the case when the primary and subsequent plastic curves are parallel to each other, in particular, we have $b = 1$ and then recover the yield strength given in (Xiao 2013).

4. Two stages beyond the pseudo-elastic stage

In this section, results will be provided for the two stages outside the pseudo-elastic stage, namely, the fast rising part between points B and C and the softening part after point C (cf., Fig. 1). These two stages will be treated separately.

4.1. Hardening stage with irrecoverable strains

The primary plastic curve is still prescribed by a shape function as shown by Eq. (14). Unlike the case in the pseudo-elastic stage, however, each subsequent plastic curve intersects the strain axis not at the origin O but at an other point O_* (cf., Fig. 1), thus leading to appreciable irrecoverable

strain upon unloading. It is expected that the latter will be growing as the unloading point H^* moves toward point C. Moreover, the shape of the subsequent plastic curve may be different from that of the counterpart in the pseudo-elastic stage.

We are going to show that the above new features may be characterized simply by introducing changes in two respects, namely, by adding a $\tilde{\kappa}-$dependent term, denoted $g = g(\tilde{\kappa})$, to the expression Eq. (28) for the yield strength and by prescribing the plastic slope of the subsequent plastic curve in a slightly modified form of Eq. (22). These changes come into play only in the hardening stage, as shown below:

$$\begin{cases} (\underline{\tau} - \underline{\alpha})\underline{\tau}' = \underline{K}(\underline{\tau}) \equiv \frac{1}{d\underline{h}/d\underline{\tau} - E^{-1}} = \frac{b_0^{-1}}{p'(b_0\underline{\tau} + d_0) - E^{-1}} \,, \\ \tilde{\kappa} > \tilde{\kappa}_0 \,, \end{cases} \tag{29}$$

for the plastic slope for the subsequent plastic curve, and

$$\begin{cases} r = \frac{g(\tilde{\kappa})}{b_0+1} + \frac{b_0-1}{b_0+1}\sqrt{1.5}\zeta + \frac{d_0}{b_0+1} \,, \\ \tilde{\kappa} > \tilde{\kappa}_0 \,, \end{cases} \tag{30}$$

for the yield strength, where $\tilde{\kappa}_0$ is the effective plastic work at point B. Moreover, the plastic slope of the primary plastic curve is given as before (cf., Eq. (21)). Now the hardening moduli c and γ are still of the same forms as those given in the last section, namely, by Eqs. (25)-(26) with Eqs. (14), (21) and (29), where the plastic slope for the subsequent plastic curve should be given by Eq. (29) and the yield strength r by Eq. (30).

Now the shape function for the subsequent plastic curve is no longer given by Eq. (16). In what follows we are in a position to derive this shape

function. Firstly, from the yield conditions at points H^* and H_*, namely,

$$\tau^* - \alpha^* = r^*\,,$$

$$\tau_* - \alpha_* = -r_*\,,$$

where $\alpha^* = \alpha_*$ and $r^* = r_*$, we deduce

$$\begin{cases} \tau_* = \tau^* - 2r^*\,, \\ \alpha^* = \tau^* - r^*\,. \end{cases} \tag{31}$$

Then, by applying the elastic equation Eq. (13) at point H_* we infer that the strain at point H_* is given by

$$h_* = p(\tau^*) - \frac{1}{E}(\tau^* - \tau_*)\,, \tag{32}$$

where $p(\tau^*)$ is the strain at the unloading point H^*. Since the plastic slope for the subsequent plastic curve is given by Eq. (29), we deduce

$$\frac{d\underline{h}}{d\underline{\tau}} = b_0\, p'(b_0\underline{\tau} + d_0) + \frac{1 - b_0}{E}\,. \tag{33}$$

This results in

$$\underline{h} = p(b_0\underline{\tau} + d_0) - p(d_0) + \frac{1 - b_0}{E}\,\underline{\tau} + h_*^p \tag{34}$$

for the subsequent plastic curve starting at point H_*, where

$$h_*^p = h_* + p(d_0) - p(b_0\tau_* + d_0) - \frac{1 - b_0}{E}\,\tau_*\,. \tag{35}$$

The latter is just the irrecoverable strain at $\underline{\tau} = 0$. By using Eqs. (30)-(32) we deduce

$$b_0\tau_* + d_0 = \tau^* - g^*\,, \tag{36}$$

$$h_*^p = p(d_0) + [p(\tau^*) - p(\tau^* - g^*)] - \frac{1}{E}(g^* + d_0)\,. \tag{37}$$

From this it follows that the term $g = g(\tilde{\kappa})$ may be given in fitting any given data for irrecoverable strains. In particular, from Eqs. (35) and (37) the meaning of the hardening term may be clear: it determines both the subsequent yield stress and the irrecoverable strain upon unloading.

4.2. Softening stage up to failure

Results for the softening stage up to failure may be given by following the main procedures in the last subsection, with changes in shape functions and plastic slopes.

In the softening stage starting at point C (cf., Fig. 1), the primary plastic curve goes invariably down toward the strain axis and, accordingly, the stress goes to asymptotically vanish, namely,

$$\lim_{\tilde{\kappa}\to\infty} \tau = 0\,. \tag{38}$$

As a result, there will be two strains corresponding with each stress τ below the maximum stress τ_s at point C. This implies that an increasing strain-stress function as shown in Eq. (14) could not cover the falling part.

With the above fact in mind, the falling part of the primary plastic curve is prescribed by a decreasing strain-stress function below:

$$\begin{cases} \overline{h} = p_s(\overline{\tau}), \quad \tilde{\kappa} > \tilde{\kappa}_s\,, \\ p_s'(\overline{\tau}) < 0\,, \\ \lim_{\overline{\tau}\to 0} p_s'(\overline{\tau}) = -\infty,\ \lim_{\overline{\tau}\to 0} p_s(\overline{\tau}) = +\infty\,. \end{cases} \tag{39}$$

Here, $\tilde{\kappa}_s$ is the effective plastic work at point C. As in Eq. (21), the plastic slope for the falling part is given by

$$(\overline{\tau} - \overline{\alpha})\,\overline{\tau}' = \overline{K}_s(\overline{\tau}) \equiv \frac{1}{p_s'(\overline{\tau}) - E^{-1}}\,. \tag{40}$$

On the other hand, the plastic slope for the subsequent plastic curve is given by

$$(\underline{\tau} - \underline{\alpha})\,\underline{\tau}' = \underline{K}_s(\underline{\tau}) \equiv \frac{1}{q_s'(\underline{\tau}) - E^{-1}} = \frac{b_s^{-1}}{p_s'(b_s\underline{\tau}) - E^{-1}} \tag{41}$$

In the above, $b_s > 0$ is a dimensionless parameter.

Now the yield strength is given by (cf., Eq. (30))

$$\begin{cases} r = \frac{g_s(\tilde{\kappa})}{b_s+1} + \sqrt{1.5}\frac{b_s-1}{b_s+1}\zeta\,, \\ g_s'(\tilde{\kappa}) < 0, \quad \lim_{\tilde{\kappa}\to+\infty} g_s(\tilde{\kappa}) = 0\,, \\ \tilde{\kappa} > \tilde{\kappa}_s\,, \end{cases} \tag{42}$$

As shown above, here $g_s = g_s(\tilde{\kappa}) > 0$ is a softening term. Moreover, the hardening moduli c and γ are given by Eqs. (24)-(26) by replacing the plastic slopes $\overline{K}(\cdot)$ and $\underline{K}(\cdot)$ in Eq. (24) with $\overline{K}_s(\cdot)$ and $\underline{K}_s(\cdot)$ given by Eqs. (40)-(41).

In the softening stage, the subsequent plastic curve starting from the subseqnent yield point (τ_*, h_*) may be derived following the same procedures in the last subsection and given by (cf., Eqs. (34) and (37))

$$\underline{h} = p_s(b_s\underline{\tau}) + \frac{1-b_s}{E}\,\underline{\tau} + \omega^* \tag{43}$$

with

$$\omega^* = [p_s(\tau^*) - p_s(\tau^* - g_s^*)] - \frac{g_s^*}{E}\,. \tag{44}$$

Here, the constant ω^* given in the above does not represent the irrecoverable strain. In fact, it follows from Eqs.(39) and (43) that, along each subsequent plastic curve, the strain becomes indefinitely large as the stress goes monotonically down to vanish, just as the case along the falling part of the primary plastic curve.

Now we study the case when $\tilde{\kappa} \to +\infty$ at failure. Let (τ_*, h_*) be the subsequent yield point corresponding with the unloading point (τ^*, h^*). Then, the following relation may be derived from Eq. (31) and Eq. $(42)_1$:

$$r^* = \frac{b_s - 1}{2b_s}\tau^* + \frac{1}{2}\frac{g_s^*}{b_s}, \tag{45}$$

$$\alpha^* = \frac{b_s + 1}{2b_s}\tau^* - \frac{1}{2}\frac{g_s^*}{b_s}, \tag{46}$$

$$\tau_* = \frac{\tau^* - g_s^*}{b_s}. \tag{47}$$

The last indicates that the softening term $g_s = g_s(\tilde{\kappa})$ determines the subsequent yield stress in the softening stage. Moreover, from Eqs. (39)-(42) and Eqs. (45)-(47) it follows that the following asymptotic properties hold true:

$$\lim_{\tilde{\kappa}\to+\infty} \tau^* = 0, \ \lim_{\tilde{\kappa}\to+\infty} \tau_* = 0, \ \lim_{\tilde{\kappa}\to+\infty} \alpha^* = 0\,,$$

$$\lim_{\tilde{\kappa}\to+\infty} \overline{K}_s = \lim_{\overline{\tau}\to 0} \overline{K}_s(\overline{\tau}) = 0, \quad \lim_{\tilde{\kappa}\to+\infty} \underline{K}_s = \lim_{\underline{\tau}\to 0} \underline{K}_s(\underline{\tau}) = 0\,,$$

and

$$\begin{cases} \lim_{\tilde{\kappa}\to+\infty} r = 0\,, \\ \lim_{\tilde{\kappa}\to+\infty} c = 0\,, \\ \lim_{\tilde{\kappa}\to+\infty} \frac{\gamma}{r} \geq \omega_0 > 0\,, \end{cases} \tag{48}$$

The latter are just the failure conditions derived in a previous study (Xiao 2014b).

5. Combining all three stages up to failure

In the last two sections, the three different deformation stages have been isolatedly treated and, therefore, results presented are merely applicable to their respective stages. In this section, such isolated results will be combined into unified results for all three stages up to failure.

5.1. Results in unified form

Toward the above objective, we introduce two hyperbolic tangent functions as follows (Xiao 2014b; Wang and Xiao 2015):

$$\pi_0 = \tanh \beta_0 \left(1 - \frac{\tilde{\kappa}}{\tilde{\kappa}_0}\right), \tag{49}$$

$$\pi_s = \tanh \beta_s \left(1 - \frac{\tilde{\kappa}}{\tilde{\kappa}_s}\right). \tag{50}$$

In the above, $\tilde{\kappa}_0$ and $\tilde{\kappa}_s$ are the effective plastic works close to points B and C (Fig. 1), respectively, and, besides, $\beta_0 > 0$ and $\beta_s > 0$ are large dimensionless parameters. The properties of these functions will be indicated slightly later.

In what follows the three constitutive quantities for all three stages will be presented in unified forms, separately. Firstly, the yield strength in unified form is given by:

$$r = \frac{\hat{g}}{\hat{b}+1} + \frac{\hat{b}-1}{\hat{b}+1}\sqrt{1.5}\zeta + \frac{\hat{d}}{\hat{b}+1} + \frac{br_0}{b+1}e^{-\beta\frac{\tilde{\kappa}}{r_0}} - \sqrt{1.5}\,\frac{b-1}{b+1}\zeta e^{-\varrho\frac{\zeta}{r_0}}, \tag{51}$$

where

$$\hat{g} = g(\tilde{\kappa})\frac{(1-\pi_0)(1+\pi_s)}{4} + g_s(\tilde{\kappa})\frac{1-\pi_s}{2}, \tag{52}$$

$$\hat{b} = \left(b\,\frac{1+\pi_0}{2} + b_0\frac{1-\pi_0}{2}\right)\frac{1+\pi_s}{2} + b_s\frac{1-\pi_s}{2}, \tag{53}$$

$$\hat{d} = \left(r_0 \frac{1+\pi_0}{2} + d_0 \frac{1-\pi_0}{2} \right) \frac{1+\pi_s}{2} \,. \tag{54}$$

For the parameters and quantities emerging in the above, refer to §3 and §4 for detail.

Next, the two moduli c and γ in unified forms are obtained following the same procedures as in obtaining Eqs. (25)-(26) and given by

$$c = \frac{K(-\zeta\overline{r}', r, \tilde{\kappa}) - rr'}{1 - \overline{r}'^2} \,, \tag{55}$$

$$\gamma = \frac{1 + \zeta^{-1}\overline{r}'\Lambda}{(1-\overline{r}'^2)(\Lambda + \overline{r}'\zeta)} (K(-\overline{r}'\zeta, r, \tilde{\kappa}) - rr') + \frac{rr' - K(\Lambda, r, \tilde{\kappa})}{\Lambda + \overline{r}'\zeta} \tag{56}$$

where (cf., Eq. (24))

$$K(\Lambda, r, \tilde{\kappa}) \equiv \frac{[\Lambda + r]}{|\Lambda| + r} \overline{K}(|\Lambda| + r, \tilde{\kappa}) + \left(1 - \frac{[\Lambda + r]}{|\Lambda| + r} \right) \underline{K}(|\Lambda| - r, \tilde{\kappa}) \tag{57}$$

with (cf., Eqs. (21)-(22))

$$\overline{K}(\overline{\tau}, \tilde{\kappa})^{-1} = p'(\overline{\tau}) \frac{1+\pi_s}{2} + p_s'(\overline{\tau}) \frac{1-\pi_s}{2} - E^{-1} \,, \tag{58}$$

$$\underline{K}(\underline{\tau}, \tilde{\kappa})^{-1} = b \left(p'(\hat{b}\underline{\tau} + \hat{d}) - \frac{1}{E} \right) \frac{1+\pi_s}{2} + b_s \left(p_s'(b_s\underline{\tau}) - \frac{1}{E} \right) \frac{1-\pi_s}{2} \,. \tag{59}$$

Now we demonstrate that the isolated results in the last two sections are indeed incorporated into the above results in unified forms. In fact, the parameters β_0 and β_s may be taken to be fairly large, say 5 or so. In this case, the two hyperbolic tangent functions given by Eqs. (49)-(50) are of the following properties:

$$\pi_0 \approx \begin{cases} +1 & \text{for } \tilde{\kappa} < \tilde{\kappa}_0(1-\epsilon) \,, \\ -1 & \text{for } \tilde{\kappa} > \tilde{\kappa}_0(1+\epsilon) \,, \end{cases} \tag{60}$$

$$\pi_s \approx \begin{cases} +1 & \text{for } \tilde{\kappa} < \tilde{\kappa}_s(1-\epsilon)\,, \\ -1 & \text{for } \tilde{\kappa} > \tilde{\kappa}_s(1+\epsilon)\,, \end{cases} \tag{61}$$

In the above, ϵ is small for fairly large β_0 and β_s. From the above properties it follows that the unified results may reduce to the isolated results separately for three stages in §3 and §4, except for two small neighborhoods at $\tilde{\kappa}_0$ and $\tilde{\kappa}_c$, separately. Within either of these two neighborhoods emerges a smooth transition between two neighboring stages.

In fact, by using Eqs. (60)-(61) we may deduce

$$\frac{1+\pi_0}{2} \approx \begin{cases} 1 & \text{for} \quad \tilde{\kappa} < \tilde{\kappa}_0(1-\epsilon)\,, \\ 0 & \text{for} \quad \tilde{\kappa} > \tilde{\kappa}_0(1+\epsilon)\,, \end{cases} \tag{62}$$

$$\frac{1-\pi_0}{2} \approx \begin{cases} 0 & \text{for} \quad \tilde{\kappa} < \tilde{\kappa}_0(1-\epsilon)\,, \\ 1 & \text{for} \quad \tilde{\kappa} > \tilde{\kappa}_0(1+\epsilon)\,, \end{cases} \tag{63}$$

$$\frac{1+\pi_s}{2} \approx \begin{cases} 1 & \text{for} \quad \tilde{\kappa} < \tilde{\kappa}_s(1-\epsilon)\,, \\ 0 & \text{for} \quad \tilde{\kappa} > \tilde{\kappa}_s(1+\epsilon)\,, \end{cases} \tag{64}$$

$$\frac{1-\pi_s}{2} \approx \begin{cases} 0 & \text{for} \quad \tilde{\kappa} < \tilde{\kappa}_s(1-\epsilon)\,, \\ 1 & \text{for} \quad \tilde{\kappa} > \tilde{\kappa}_s(1+\epsilon)\,, \end{cases} \tag{65}$$

Thus, for the first stage with $\tilde{\kappa} < \tilde{\kappa}_0$ and the second stage with $\tilde{\kappa}_0 < \tilde{\kappa} < \tilde{\kappa}_s$ and $\tilde{\kappa} > \tilde{\kappa}_s$ for the softening stage, it follows from Eqs. (52)-(59) and Eqs. (62)-(65) that Eq. (51) and Eqs. (55)-(56) reduce to the results in §3 and §4, separately.

5.2. Determination of the shape function

In the unified results presented, the constitutive quantities except β_0 and β_s are obtainable from relevant data for the three deformation stages by means of uncoupled procedures, as indicated in the last two sections. These quantities are expressed explicitly in terms of uniaxial shape functions for the primary and subsequent plastic curves and apply to a general case of multi-axial deformations. As such, the finite elastoplastic J_2-flow models established in §2 may simultaneously represent all three deformation stages of pseudo-elastic SMAs over the entire range of strain up to failure. Perhaps more essentially, the proposed model is explicit in the following sense, namely, *both the primary and the subsequent plastic curves determined from this model in respective deformation stages are nothing else but exactly those prescribed by the shape functions therein incorporated. As a result, the proposed model may automatically fit any given test data for such curves, whenever suitable forms of shape functions may be chosen to fit any given data.* The implication of this respect will further be explained in the concluding section.

Now a comprehensive simulation of pseudo-elastic SMAs up to failure becomes explicit and straightforward and may be reduced to prescribing the shape functions from relevant uniaxial data, among other things. It is noted that the shape function eq. (14) may be presented to precisely fit any given data for any shape of the loading curve ABC in Fig. 1. In fact, let $(\overline{h}_s, \overline{\tau}_s)$ with $s = 1, 2, \cdots, N$ be any given set of data for the axial stress and strain. The shape function eq. (14) may be given straightforwardly by the interpo-

lating polynomial below:

$$\overline{h} = p(\overline{\tau}) = \sum_{s=1}^{N} \overline{h}_s L_s(\overline{\tau}) \,,$$

where

$$L_s(\overline{\tau}) = \prod_{r=1\neq s}^{N} \frac{\overline{\tau} - \overline{\tau}_r}{\overline{\tau}_s - \overline{\tau}_r} \,, \quad s = 1, 2, \cdots, N \,,$$

are the Lagrangean base functions. Then,

$$p(\overline{\tau}_s) = \overline{h}_s, \quad s = 1, 2, \cdots, N \,.$$

Thus, the test data given are precisely fitted.

The interpolating approach as shown above is straightforward with no adjustable parameters and apples to any given data. Another approach is to prescribe certain well-chosen forms of shape functions with certain parameters associated with direct geometric and physical features of SMA stress-strain curves. Such parameters are determined in fitting test data.

Unlike the interpolating approach, the latter approach involves procedures of parameter identification and need not be applicable for all cases. However, this approach may supply parameters characterizing typical geometrical and physical features of SMAs. Detail will be shown in the next section.

6. Numerical examples for comprehensive simulation

In this section, we are going to present numerical examples for simulating all three stages of SMAs up to failure. As indicated before, with the proposed model it suffices to supply two shape functions (cf., Eqs. (15)-(16)) that can

match test data for primary and subsequent plastic curves. Toward this goal, the second approach indicated at the end of the last section will be adopted below.

6.1. Shape functions for SMAs with flag-like hysteresis loops

Pseudo-elastic hysteresis loops for SMAs, in particular, Ti-Ni alloys, are of flag-like shape, as shown in Fig. 1. The main features of such loops may be sketchily described as follows. For the primary stress-strain curve, after an initial almost linear part with a big slope follows an almost linear part with a small slope in the pseudo-elastic stage and then a rising part in the hardening stage, and, moreover, within small intervals there are smooth transitions between neighboring parts. In an unloading process of removing the stress, the stress-strain curve displays similar features as just described.

It has been shown (Xiao 2013, 2014a) that two simple forms of shape functions may be introduced to capture the main features in the foregoing and given by

$$\begin{cases} \overline{h} & = \frac{r_0}{E} + \xi_0(\overline{\tau} - r_0) + \\ & \quad + \frac{1}{2}(a\overline{\tau}^2 + \xi_1(\overline{\tau} - r_0 - s) + a_0)\left(\tanh(m(\overline{\tau} - r_0 - s)) + \tanh(ms)\right) , \end{cases} \tag{66}$$

for the primary plastic curve, and

$$\begin{cases} \underline{h} & = (\xi_0 b + (1-b)E^{-1})\ \underline{\tau} + \\ & \quad + \frac{1}{2}(a(b\underline{\tau} + r_0)^2 + \xi_1(b\,\underline{\tau} - s) + a_0)\left(\tanh(m(b\,\underline{\tau} - s)) + \tanh(ms)\right) , \end{cases} \tag{67}$$

for the subsequent plastic curve. The latter is obtained from Eqs. (15)-(17). All the nine parameters therein are intrinsic in the sense of representing intrinsic geometric features of loops, as explained in the foregoing references.

The above shape functions are for the first, i.e., the pseudo-elastic stage with perfect recovery. For the second, i.e., the hardening stage with partial recovery, the shape function for the primary plastic curve is still given by Eq. (66), while the shape function for the subsequent plastic curve is given by Eq. (34) with Eq. (37). The shape function for the falling part (cf., Eq. (39)) is given by

$$\overline{h} = p_s(\overline{\tau}) = h_s \left[1 + \left(-\frac{1}{\lambda_s} \ln \frac{\overline{\tau}}{\tau_s} \right)^a \right], \; 0 < \overline{\tau} \leq \tau_s \,, \tag{68}$$

where h_s and τ_s are the strain and the stress at point C (Fig. 1) and $n > 0$, $a > 0$ and $\lambda_s > 0$ are dimensionless parameters.

With suitable values of the parameters $\tilde{\kappa}$ and β_s, the falling part in the softening stage up to failure should be determined by numerically integrating the rate constitutive equations with the yield strength r and the hardening moduli c and γ given by Eqs. (42)-(44). That is also the case for the smooth transitions from the first to the second stage and from the second to the third stage.

It may be straightforward to fit relevant test data using the above shape functions. This may be done by directly finding out the parameters incorporated. As has been indicated before, usual tedious numerical procedures in treating nonlinear constitutive equations are now rendered irrelevant.

6.2. Numerical results

Numerical results incorporating the test data in Shaw and Kyriakides (1995) are now presented. Of them, data in the second stage with partial recovery are provided for one subsequent plastic curve. The irrecoverable strain in this case may be determined and denoted h^p_*, as has been done in Eq. (34).

It should be noted that the strain in Fig. 5 in Shaw and Kyriakides (1995) represents the average strain in the monitored gauge length of the wire sample. The deformation response in the tested sample is inhomegeneous due to austenitic phase showing Lüders band-like localization during forward and reverse martensitic transformation, as elaborated in Shaw and Kyriakides (1995, 1997, 1998) and Hallai and Kyriakides (2013).

Results will be presented below for three stages, separately. Firstly, the parameters in the two shape functions in Eqs. (66)-(67) are identified in fitting the data for the pseudo-elastic hysteresis loop (Shaw and Kyriakides 1995) and given by

$$E = 60\text{GPa},\ r_0 = 266\text{MPa},\ \xi_0 = 1.5\times 10^{-5}/\text{MPa},\ a = 1.0\times 10^{-8}/\text{MPa}^2,$$

$$\xi_1 = 1.6\times 10^{-5}/\text{MPa},\ s = 280\text{MPa},\ a_0 = 3.7\times 10^{-2},\ m = 0.2,\ b = 0.95.$$

Moreover, the effective plastic work $\tilde{\kappa}_{00}$ at the first unloading point may be obtained by integrating Eq. (21) with $\overline{\tau} - \alpha = r$ from $\overline{\tau} = r_0 = 266$MPa to $\overline{\tau} = 720$MPa and given by

$$\tilde{\kappa}_{00} = 6.07\text{MPa}.$$

Results are shown in Fig. 2.

Secondly, the parameters b_0, d_0 and h_*^p are determined in fitting the data for the subsequent plastic curve in the second stage (Shaw and Kyriakides 1995) and given by

$$b_0 = 1,\ d_0 = 620\text{MPa},\ h_*^p = 6.3 \times 10^{-2}.$$

Again, the effective plastic work $\tilde{\kappa}^*$ at the second unloading point is obtained by integrating Eq. (29) with $\overline{\tau} - \alpha = r$ from $\overline{\tau} = 720$MPa to $\overline{\tau} = 1407$MPa and, besides, the value $g^* = g(\tilde{\kappa}^*)$ is obtained from Eq. (37) with $\tau^* = 1407$MPa, as given below:

$$\tilde{\kappa}^* = 31.26\text{MPa}, \quad g^* = 321.8\text{MPa}.$$

Here, for the sake of simplicity the hardening term $g = g(\tilde{\kappa})$ in Eq. (30) is taken to be of the linear form given below:

$$g = \frac{g^*}{\tilde{\kappa}^*}\tilde{\kappa} = 0.2287\tilde{\kappa}\,. \tag{69}$$

Results are shown in Fig. 3.

Thirdly, the falling part of the curve in the softening stage in case of monotonic straining up to failure is generated by the shape function given by Eq. (68) with

$$h_s = 0.125,\ \tau_s = 1700\text{MPa},\ \lambda_s = 6.$$

Moreover, the softening curve in case of unloading is produced by Eqs. (43), (44), (47) and (68) with

$$\tau^* = 1185\text{MPa},\ b_s = 1.5,\ \omega^* = -2.65,\ g_s^* = 495\text{MPa},\ \tau_* = 460\text{MPa}.$$

Results are shown in Fig. 4.

The above results are combined into Fig. 5 to display a comprehensive simulation of all three stages up to failure. The four figures show good agreement with test data.

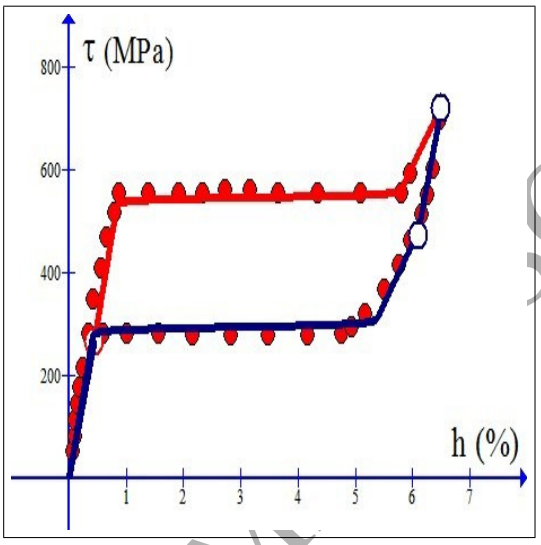

Figure 2: Fitting test data (solid points, Shaw and Kyriakides 1995) in the pseudo-elastic stage with perfect strain recovery

Details may further be given for smooth transitions from the first to the second stages and from the second to the third stage, which occurs in two small intervals $(\tilde{\kappa}_0(1-\epsilon), \tilde{\kappa}_0(1+\epsilon))$ and $(\tilde{\kappa}_s(1-\epsilon), \tilde{\kappa}_s(1+\epsilon))$, separately. It may be noted that the transition from the first to the second stage is characterized by the two parameters $\tilde{\kappa}_0$ and β_0 (cf. Eq. (49)), while that from the second to the third stage is described by the two parameters $\tilde{\kappa}_s$ and β_s (Ed. (50)). With a lack of relevant data, here estimated values of these

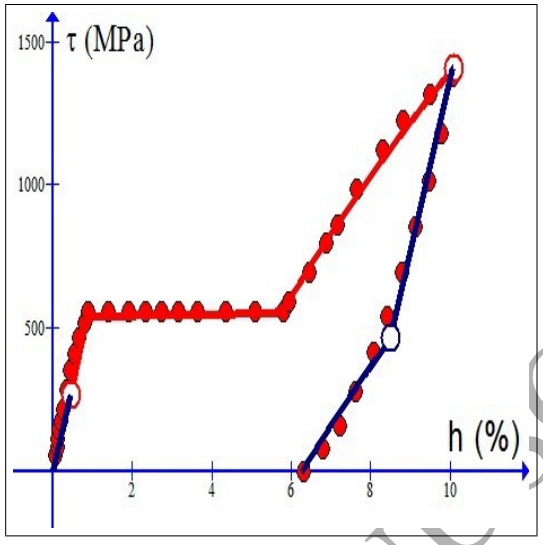

Figure 3: Fitting test data (solid points, Shaw and Kyriakides 1995) in the hardeing stage with partial strain recovery

parameters are taken into consideration, e.g.,

$$\kappa_0 = 7\text{MPa}, \quad \beta_0 = 21,$$

$$\tilde{\kappa}_s = 70\text{MPa}, \quad \beta_s = 21.$$

Moreover, here the softening term $g_s = g_s(\tilde{\kappa})$ in Eq. (42) is taken to be of the simple form:

$$g_s = g^* \frac{\tilde{\kappa}^0}{\tilde{\kappa}^*} \frac{\tilde{\kappa}^0}{\tilde{\kappa}} \,. \tag{70}$$

Note that both g and g_s agree with each other at $\tilde{\kappa} = \tilde{\kappa}^0$.

Results for the foregoing two transitions may be obtained by integrating the constitutive equations in §2 with the yield strength and hardening moduli in unified form.

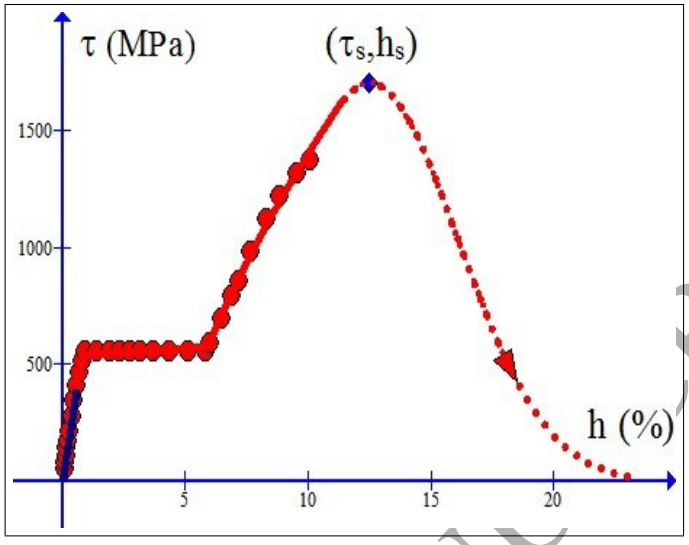

Figure 4: Monotonic straining up to failure with test data (solid points, Shaw and Kyriakides 1995; broken line for softening part).

In the numerical examples given in the above, test data are only for part of the second irrecoverable stage and no data for the sofening part up to failure is involved, as may be seen in Fig. 4. Toward further validating the shape function Eq. (66) prior to the softening and the shape function Eq. (68) for the sofening part, test data given in Fig. 2(a) in Gollerthan et al. (2009) and in Fig. 2 in Giroux et al (2010) for the strain rate $2.5\times10^{-4}/s$ are taken into consideration, separately. In the former, complete data are given for the first two stages of a SMA sample except the softening stage, while data incorporating the softening stage are given in the latter. Results in simulating these two sets of data are given below.

For the data in Gollerthan et al. (2009), the parameter values are as

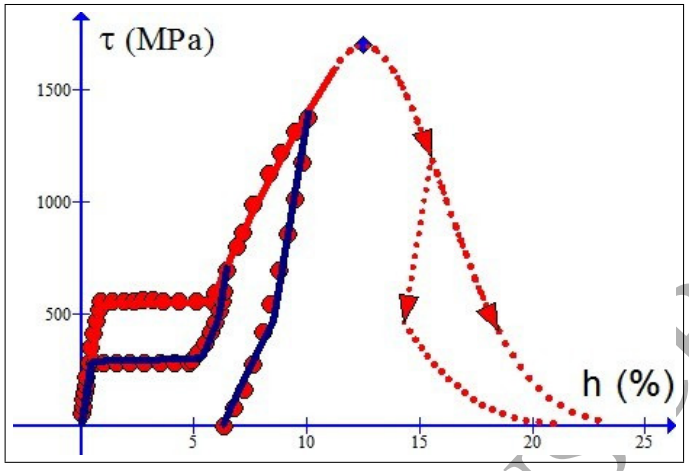

Figure 5: Comprehensive simulation of three stages up to failure with test data (solid points, Shaw and Kyriakides 1995; upper broken line for softening part in case of monotonic straining; lower broken line for softening part in case of unloading)

follows:

$$r_0 = 100\text{MPa},\ E = 5\text{GPa},\ \xi_0 = 2.2 \times 10^{-4}/\text{MPa},\ a = 4.0 \times 10^{-7}/\text{MPa}^2,$$

$$\xi_1 = 1.5 \times 10^{-5} \times /\text{MPa},\ s = 110\text{MPa},\ a_0 = 0.0545,\ m = 0.2/\text{MPa},$$

for the shape function eq. (66), and

$$h_s = 0.67,\ \tau_s = 960\text{MPa}\ \ \lambda_s = 2,\ d = 2,$$

for the shape function Eq. (68) for the softening stage. The simulation result is shown in Fig. 6.

Moreover, for the data in Giroux et al. (2010), the parameter values are given by

$$r_0 = 330\text{MPa},\ E = 100\text{GPa},\ \xi_0 = 1.25 \times 10^{-5},\ a = 0,$$

$$\xi_1 = 0,\ s = 96\text{MPa},\ a_0 = 16,\ m = 0.15/\text{MPa},$$

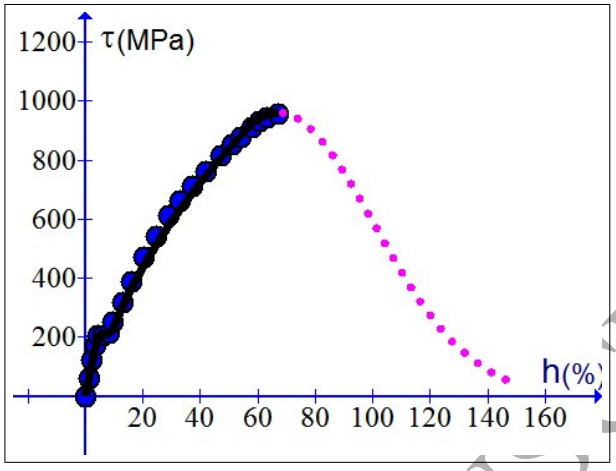

Figure 6: Fitting test data (solid points, Gollerthan et al. 2009) up to failure

for the shape function eq. (66) for the first two stages, and

$$h_s = 0.06,\ \tau_s = 424\text{MPa}\ \lambda_s = 0.032,\ d = 3.06,$$

for the shape function Eq. (68) for the softening stage. The simulation result is shown in Fig. 7.

7. Concluding remarks

In the previous sections, a new constitutive model for pseudo-elastic SMAs up to failure has been proposed in the framework of classical J_2-flow elastoplasticity. The new model accomplishes for the first time a comprehensive simulation of all three stages over the entire range of strain. In comparison with various usual models, the new model exhibits new features in an explicit, unified sense as explained below.

(i) With each usual model, complexities in two respects would have to be treated. Firstly, a number of adjustable constitutive parameters and func-

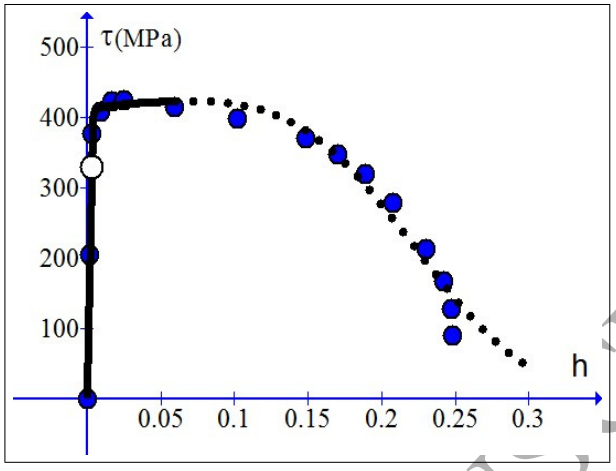

Figure 7: Fitting test data (solid points, Giroux et al. 2010) up to failure

tions from either microscopic or mesoscopic or phenomenological standpoint are incorporated in both nonlinear constitutive equations and switching conditions as well as micro-to-macro averaged procedures. Given values of such parameters and forms of such functions, model predictions for both the primary plastic curve upon loading and each subsequent plastic curve upon unloading may not be explicitly obtainable but, on the contrary, would have to be found by means of numerical procedures of treating a coupled system of nonlinear constitutive equations with a number of switching conditions and micro-to-macro averaging procedures.

(ii) Secondly, for data sets given for a certain SMA sample, such numerical procedures would have to be iteratively carried out until suitable values of constitutive parameters and forms of constitutive functions may be found to fit such data sets as closely as possible. In so doing, much effort and complexity in numerical treatment would be expected.

(iii) The applicability of a model can be validated for given data sets for

a sample only after the foregoing process is favorably completed. Even if a model has been validated for a sample, however, there would be no certainty that that may be the case for any other sample. For different SMA samples, the foregoing process would have to be repeated one by one and give rise to different results for both constitutive parameters and functions for different samples. As such, it may be evident that the validation of a model not only could never be completed by exhausting all possible samples, but could not supply results in unified form.

(iv) The complexities and, in particular, the uncertainty as indicated above may be bypassed with the new model proposed. In fact, both the yield strength and the hardening moduli presented in §5 are explicitly expressed in terms of any given shape functions for the primary and subsequent plastic curves, in such a sense that the latter two may be exactly, automatically reproduced from the model. As a consequence, with the proposed model, the modeling of pseudo-elastic SMAs up to failure may substantially be reduced to choosing suitable forms of shape functions, thus bypassing usual complicated numerical procedures indicated above. In fact, as explained in §5.2, it may be a straightforward matter to obtain the shape function by means of interpolating procedures. Since explicit results in unified form are presented in terms of any form of the shape function and the latter can prescribe any given shape of uniaxial stress-strain, it may be clear that the proposed model provides a unified means of simulating SMAs, in an explicit sense of accurately fitting any given uniaxial test data.

On the other hand, the particular forms of the shape functions as given by eqs. (66)-(68) are intended for NiTi SMAs with flag-like recovery loops. In

this case, procedures of parameter identification are indeed involved. However, the parameters incorporated in these functions may be determined by directly fitting these functions to test data, without involving the complicated procedures indicated in (i) and (ii).

(v) It may follow from the above that the proposed model supplies unified results for all possible shapes of uniaxial stress-strain curves, in an explicit sense without involving both phase variables and usual complicated procedures as indicated in the above.

It should be pointed out that the above discussion is concerned with determination of the constitutive quantities and parameters based on uniaxial test data. Whenever the model is ready, responses in multi-axial cases should be calculated by means of usual numerical procedures for 3-dimmensional problems of elastoplastic bodies.

From the above explanations it may be concluded that the novelty of the new model lies not only in achieving for the first time a comprehensive simulation up to failure, but, perhaps more essentially, in presenting explicit, unified results in terms of two shape functions and others. Developments may be expected in the four respects indicated below.

Firstly, the pseudoelasticity behavior and fatiguing failure under repeated loadings need to be studied. This will be done by combining the new model here with the free, smooth elastoplasticity model suggested in a newest study (Xiao et al. 2014; Xiao 2014b; Wang and Xiao 2015).

Secondly, rate effects need be considered in many cases. A new rate-dependent elastoplasticity model has been established most recently (Xiao 2015). With this development, the new model here will be extended to treat

rate effects in various cases.

Thirdly, SMA samples are known to exhibit distinct behaviors over different ranges of temperature. The pseudo-elastic behavior is observed and changes over a certain range of temperature. Outside this range, usual elasto-plastic behavior is observed over the whole range of strain. A thermo-coupled model for SMAs need be established to simulate such distinct behaviors over the whole range of temperature. This will be done by extending the new model here to thermo-coupled cases.

Finally, since phase transitions between austenite and martensite at the microscopic level are the physical mechanisms of SMA macroscopic behavior, it may be of significance to establish links between these mechanisms and the macroscopic constitutive quantities in the proposed model, namely, the yield strength and the hardening moduli. An initial understanding of these links may be evident. In fact, both phases and phase boundaries at the microscopic level are undergoing constant changes in course of phase transitions. As such, transitions between different phases may result in appreciable change in the yield strength, while interactions between changing phase boundaries may lead to strong anisotropic hardening effect. On account of the fact that changes in phases and in associated phase boundaries are coupled with each other, there exists substantial coupling between the foregoing two kinds of hardening effects, as is the case in the proposed model. Quantitative links in a further sense need to be studied.

Acknowledgments

This work was carried out under the joint support of the funds from Natural Science Foundation of China (No.: 11372172), from the 211-project launched by the Education Committee of China through Shanghai University (No.: S.15-0303-15-208) and from the science and technology development project lauched by Weifang municipal government (No.: 2015GX018).

References

References

[1] Arghavani, J., Auricchio, F., Naghdabadi, R., Reali, A., Sohrabpour, S., 2010a. A 3-D phenomenological constitutive model for shape memory alloys under multi-axial loadings. Int. J. Plasticity 26, 976-991.

[2] Arghavani, J., Auricchio, F., Naghdabadi, R., Reali, A., Sohrabpour, S., 2010b. A 3D finite strain phenomenological constitutive model for shape memory alloys considering martensite reorientation. Continuum Mech. Thermodyn., DOI 10.1007/s00161-010-0155-8.

[3] Arghavani, J., Auricchio, F., Naghdabadi, R., Reali, A., Sohrabpour, S., 2011. A finite strain kinematic hardening constitutive model based on Hencky strain: General framework, solution algorithm and application to shape memory alloys. Int. J. Plasticity 27, 976-991.

[4] Auricchio, F., 1995. Shape Memory Alloys: Applications, Micromechanics and Numerical Simulations. University of California, Berkley.

[5] Auricchio, F., 2001. A robust integration-algorithm for a finite-strain shape-memory-alloy superelastic model. Int. J. Plasticity 17, 971-990.

[6] Auricchio, F., Reali, A., Stefanelli, U., 2007. A three-dimensional model describing stress-induced solid phase transformation with permanent inelasticity. Int. J. Plasticity 23, 207-226.

[7] Auricchio, F., Taylor, R.L., 1997. Shape-memory alloys: modelling numerical simulations of the finite-strain superelastic behavior. Compt. Meth. Appl. Mech. Eng. 143, 175-194.

[8] Battacharya, K., 2003. Microstructure of Martensite: Why It Forms and How It Gives Rise to the Shape Memory Effect. Oxford University Press, Oxford.

[9] Brocca, M., Brinson, L.C., Bazant, Z.P., 2002. Three-dimensional constitutive model for shape memory alloys based on microplane model. J. Mech. Phys. Solids 50, 1051-1077.

[10] Bruhns, O. T., Xiao, H., Meyers, A., 1999. Self-consistent Eulerian rate type elasto-plasticity models based upon the logarithmic stress rate. Int. J. Plasticity 15, 479–520.

[11] Bruhns, O. T., Xiao, H., Meyers, A., 2003. Some basic issues in traditional Eulerian formulations of finite elastoplasticity. Int. J. Plasticity 19, 2007-2026.

[12] Bruhns, O. T., Xiao, H., Meyers, A., 2005. A weakened form of Ilyushin's postulate and the structure of self-consistent Eulerian finite elastoplasticity. Int. J. Plasticity 21, 199–219.

[13] Desindes S., Daly S., 2010. The small-scale yielding of shape memory alloys under mode III fracture.Int. J. Solids Structures 47, 730-737

[14] Falk, F., 1980. Model free-energy, mechanics and thermodynamics of shape memory alloys. Acta Metallurgica 28, 1773-1780.

[15] Feng, X.Q., Sun, Q.P., 2007. Shakedown analysis of shape memory alloy structures. Int. J. Plasticity 23, 183-206.

[16] Giroux P., Dalle F., Sauzay M., Malaplate J., Fournier B., Gourgues-Lorenzon A., 2010. Mechanical and microstructural stability of p92 steel under uniaxial tension at high temperature. Mater Sci Engng A 527, 39843993.

[17] Gollerthan S., Young M.L., Baruj A., Frenzel J., Schmahl W.W., Eggeler, G., 2009. Fracture mechanics and microstructure in NiTi shape memory alloys. Acta Materialia 57, 1015-1025.

[18] Hallai,J.F., Kyriakides, S., 2013. Underlying material response for Lders-like instabilities. Int. J. Plasticity 47, 1-12.

[19] Hartl, D.J., Chatzigeorgiou, Lagoudas, D.C., 2010. Three-dimensional modeling and numerical analysis of rate-dependent irrecoverable deformation in shape memory alloys. Int. J. Plasticity 26, 1485-1507.

[20] Hartl, D.J., Lagoudas, D.C., 2009. Constitutive modeling and structural analysis considering simultaneous phase transformation and plastic yield in shape memory alloys. Smart Mater. Struct.18, 104017-104033.

[21] Helm, D., 2007. Thermomechanics of martensitic phase transitions in shape memory alloys I: constitutive theories for small and large deformations. Journal of Mechanics of Materials and Structures 2, 87-112.

[22] Helm, D., Haupt, P., 2003. Shape memory behavior: modelling within continuum mechanics. Int. J. Solids Structures 40, 827-849.

[23] Huo, Y.Z., 1989. A mathematical model for the hysteresis in shape memory alloys. Continuum Mech. Thermodyn. 1, 283-303.

[24] Khan, A.S., Huang, S.J., 1995. Continuum Theory of Plasticity. John Wiley & Sons, New York.

[25] Lagoudas, D.C., 2008. Shape Memory Alloys: Modeling and Engineering Applications. Springer, New York.

[26] Lagoudas, D.C., Entchev, P.B., Popov, P., Patoor, E., Brinson, L.C., Gao, X., 2006. Shape memory alloys, part II: modeling of polycrystals. Mechanics of Materials 38, 430-462.

[27] Lagoudas, D.C., Hartl, D., Chemisky, Y., Machado, L., Popov, P., 2012. Constitutive model for the numerical analysis of phase transformation in polycrystalline shape memory alloys. Int. J. Plasticity 32, 155-183.

[28] Lexcellent, Ch., Boubakar, M.L.,Bouvet, Ch., Calloch S., 2006.About modelling the shape memory alloy behavior based on the phase transformation surface identfication under proportional loading and anisothermal conditions.International Journal of Solids and Structures 43, 613-626

[29] Luig, P., Bruhns, O.T., 2008. On the modeling of shape memory alloys using tensorial internal variables. Mat. Sci. Eng. A481-482, 379-383.

[30] Maletta, C., Furgiuele F., 2011. Fracture control parameters for NiTi based shape memory alloys.Int. J. Solids Structures 48, 1658-1664

[31] Masud, A., Panahandeh, Auricchio, F., 1997. A finite-strain finite element model for the pseudo-elastic behavior of shape memory alloys. Comput. Meth. Appl. Mech. Engng. 148, 23-37.

[32] Mehrabi,R., Kadkhodaei,M., Elahinia M., 2014.A thermodynamically-consistent microplane model for shape memory alloys. Int. J. Solids Structures 51, 2666-2675

[33] Morin, C., Moumni, Z., Zaki, W., 2011. A constitutive model for shape memory alloys accounting for thermomechanical coupling. Int. J. Plasticity 27, 748-767.

[34] Moumni, Z., Zaki, W., Nguyen, Q.S., 2008. Theoretical and numerical modeling of solid-solid phase change: Application to the description of the thermomechanical behavior of shape memory alloys. Int. J. Plasticity 24, 614-645.

[35] Müller, Ch., Bruhns, O.T., 2006. A thermodynamic finite-strain model for pseudo-elastic shape memory alloys. Int. J. Plasticity 22, 1658-1682.

[36] Paiva,A., Savi, M.A., Braga, A., Pacheco P., 2005. A constitutive model for shape memory alloys considering tensile-compressive asymmetry and plasticity. Int. J. Solids Structures 42, 3439-3457

[37] Panico, M., Brinson, L.C., 2007. A three-dimensional phenomenological model for martensite reorientation in shape memory alloys. J. Mech. Phys. Solids 55, 2491-2511.

[38] Patoor, E., Lagoudas, D.C., Entchev, P., Brinson, L.C., Gao, X., 2006. Shape memory alloys, part I: general properties and modeling of single crystals. Mechanics of Materials 38, 391-429.

[39] Peng, X., Pi, W., Fan, J., 2008. A microstructure-based constitutive model for the pseudo-elastic behavior of NiTi SMAs. Int. J. Plasticity 24, 966-990.

[40] Peng, X.,Yang,Y., Huang, S., 2001. A comprehensive description for shape memory alloys with a two-phase constitutive model. Int. J. Solids Structures 38, 6925-6940.

[41] Popov, P., Lagoudas, D.C., 2007. A 3-D constitutive model for shape memory alloys incorporating pseudoelasticity and detwinning of self-accommodated martensite. Int. J. Plasticity 23, 1679-1720.

[42] Reese, S., Christ, D., 2008. Finite deformation pseudo-elasticity of shape memory alloys-Constitutive modelling and finite element implementation. Int. J. Plasticity 24, 455-482.

[43] Saleeb, A.F., Padula II, S.A., Kumar, A., 2011. A multi-axial multi-mechanism based constitutive model for the comprehensive representation of the evolutionary response of SMAs under general thermomechanical loading conditions. Int. J. Plasticity 27, 655-687.

[44] Shaw J.A., 2002.A thermodynamical model for a 1-D shape memory alloy wire with propagating instabilities.Int. J. Solids Structures 39, 1275-1305

[45] Shaw, J.A., Kyriakides, S.,1995. Thermomechanical aspects of NiTi. J. Mech. Phys. Solids 43, 1243-1281.

[46] Shaw, J.A., Kyriakides, S., 1997. On the nucleation and propagation of phase transformation fronts in a NiTi alloy. Acta Materialia 45, 683-700.

[47] Shaw, J.A., Kyriakides, S., Initiation and propagation of localized deformation in elastoplastic strips under uniaxial tension. Int. J. Plasticity 13, 837-871.

[48] Tanaka, K., Kobayashi, S., Sato, Y., 1986. Thermodynamics of transformation pseudoelasticity and shape memory effect in alloys. Int. J. Plasticity 2, 59-72.

[49] Tanaka, K., Nagaki, S., 1982. A thermomechanical description of materials with internal variables in the process of phase transitions. Arch. Appl. Mech. 51, 287-299.

[50] Teeriaho, J.-P., 2013. An extension of a shape memory alloy model for large deformations based on an exactly integrable Eulerian rate formulation with changing elastic properties. Int. J. Plasticity 43, 153-176.

[51] Thamburaja, P., 2010. A finite-deformation-based phenomenological theory for shape-memory alloys. Int. J. Plasticity 26, 1195-1219.

[52] Vidyashankar R.B., Khandelwal A., 2007. Differential and integrated form consistency in 1-D phenomenological models for shape memory alloy constitutive behavior.Int. J. Solids Structures 44, 4369-4381.

[53] Wang, X.M., Wang, Z.L., Xiao, H., 2014. SMA pseudo-elastic hysteresis with tension-compression asymmetry: explicit simulation based on elastoplasticity models. Continuum Mech. Thermodyn. 27, 959-970.

[54] Wang, Z.L., Xiao, H., 2015. A study of metal fatigue failure as inherent features of elastoplastic constitutive equations. In: Holm Altenbach, Tetsuya Matsuda, Dai Okumura (eds.), From Creep Damage Mechanics to Homogenization Methods - A Liber Amicorum to celebrate the brithday of Nobutada Ohno, Advanced Structural Materials 64, pp. 529-540, Springer, Berlin.

[55] Xiao, H., 2013. Pseudo-elastic hysteresis out of recoverable finite elastoplastic flows. Int. J. Plasticity 41, 82-96.

[56] Xiao, H., 2014a. An explicit, straightforward approach to modeling SMA pseudo-elastic hysteresis. Int. J. Plasticity 53, 228-240.

[57] Xiao, H., 2014b. Thermo-coupled elastoplasticity model with asymptotic loss of the material strength. Int. J. Plasticity 63, 211-228.

[58] Xiao, H., 2015. An explicit, direct simulation of multi-axial finite strain inelastic behavior for polymeric solids. Int. J. Plasticity 71, 146-169.

[59] Xiao, H., Bruhns, O. T., Meyers, A., 1997. Logarithmic strain, logarithmic spin and logarithmic rate. Acta Mechanica 124, 89–105.

[60] Xiao, H., Bruhns, O. T., Meyers, A., 2000a. The choice of objective rates in finite elastoplasticity: general results on the uniqueness of the logarithmic rate. Proc. Roy. Soc. London A 456, 1865–1882.

[61] Xiao, H., Bruhns, O. T., Meyers, A., 2000b. A consistent finite elastoplasticity theory combining additive and multiplicative decomposition of the stretching and the deformation gradient. Int. J. Plasticity 16, 143-177.

[62] Xiao, H., Bruhns, O. T., Meyers, A., 2006. Elastoplasticity beyond small deformations. Acta Mechanica 182, 31–111.

[63] Xiao, H., Bruhns, O. T., Meyers, A., 2007. Thermodynamic laws and consistent Eulerian formulations of finite elastoplasticity with thermal effects. J. Mech. Phys. Solids 55, 338–365.

[64] Xiao, H., Bruhns, O. T., Meyers, A., 2010a. Finite elastoplastic J_2-flow models with strain recovery effects. Acta Mechanica 210, 13-25.

[65] Xiao, H., Bruhns, O. T., Meyers, A., 2010b. Phenomenological elastoplasticity view on strain recovery loops characterizing shape memory materials. ZAMM-J. Appl. Math. Mech. 90, 544-564.

[66] Xiao, H., Bruhns, O. T., Meyers, A., 2011. Thermo-induced plastic flows and shape memory effects. Theoretical and Applied Mechanics 38, 155-207.

[67] Xiao, H., Bruhns, O.T., Meyers, A., 2014, Free rate-independent elastoplastic equations. ZAMM-J. Appl. Math. Mech. 94, 461-476.

[68] Yoo, Y.-I, Kim, Y.-J., Shin,D.K., Lee J.J., 2015.Development of martensite transformation kinetics of NiTi shape memory alloys under compression.International Journal of Solids and Structures 64-65, 51-61

[69] Yu, C., Kang,G.Z., Kan, Q.H., 2014a. Crystal plasticity based constitutive model of NiTi shape memory alloy considering different mechanisms of inelastic deformation. Int. J. Plasticity 54, 132-162.

[70] Yu, C., Kang G.Z., Kan Q.H. 2014b.Study on the rate-dependent cyclic deformation of super-elastic NiTi shape memory alloy based on a new crystal plasticity constitutive model.Int. J. Solids Structures 51, 4386-4405

[71] Yu, C., Kang, G.Z., Kan, Q.H., Song, D, 2013. A micromechanical constitutive model based on crystal plasticity for thermo-mechanical cyclic deformation of NiTi shape memory alloys. Int. J. Plasticity, DOI 10.1016/j.ijplas.2013.01.001.

[72] Zaki, W., 2012. An efficient implementation for a model of martensite reorientation in martensitic shape memory alloys under multiaxial non-proportional loading. Int. J. Plasticity 37, 72-94.

[73] Zhou, B., 2012. A macroscopic constitutive model of shape memory alloy considering plasticity. Mechanics of Materials 48, 71-81.

[74] Ziólkowski, A., 2007. Three-dimensional phenomenological thermodynamic model of pseudoelasticity of shape memory alloys at finite strains. Continuum Mech. Thermodyn. 19, 379-398.